


On the influence of the amorphous phase on the stability of crystals in poly(cis-1,4-isoprene) networks

Dominik Segiet | Sebastian Weckes | Juergen Austermuehl | Joerg C. Tiller | Frank Katzenberg 

Biomaterials & Polymer Science,
Department of Biochemical and Chemical
Engineering, Technische Universitat
Dortmund, Dortmund, Germany

Correspondence

Frank Katzenberg, Biomaterials &
Polymer Science, Department of
Biochemical and Chemical Engineering,
TU Dortmund, 44221 Dortmund,
Germany.
Email: frank.katzenberg@tu-dortmund.de

Abstract

Crosslinked natural rubber and synthetic rubber samples are additivated with up to 9 wt% stearic acid (StA) to better understand the influence of StA on the melting temperature T_m of strain-induced crystallized poly(cis-1,4-isoprene) crystals. To this end, lamellae thicknesses are determined from wide-angle x-ray patterns and used to calculate the crystal size dependent melting temperature $T_{m,calc}$. Comparing the measured T_m with $T_{m,calc}$ reveals that T_m deviates downward from $T_{m,calc}$ and converges $T_{m,calc}$ with increasing StA concentration until it is identical to $T_{m,calc}$, in case of room temperature strain-induced crystallization. In case of strain-induced crystallization at 80°C, it was found that T_m is identical with $T_{m,calc}$ without added StA and deviates upward from $T_{m,calc}$ with increasing amount of added StA. We suggest that this is due to internal stress onto the polymer crystals exerted by highly strained macromolecules in the surrounding amorphous phase. Whether this stress has a stabilizing or destabilizing effect on the crystals is assumed to depend on its intensity and direction, which can be efficiently altered by the amount and the location of StA crystals in the amorphous phase.

KEYWORDS

crystallization, morphology, rubber

1 | INTRODUCTION

Crystallization is an essential feature for most high-performance polymers. Even when comprised of perfectly constituted chains, polymers are not capable of crystallizing to an extent of 100%. This is due to, for example, entanglements, a more or less broad polydispersity of the macromolecular ensemble, as well as configurative faults along the macromolecular backbone.¹ For the same reasons, polymer crystals are strongly limited in size and remain in the nanoscale along at least one dimension.

Thus, surface-to-volume ratios play a major role regarding the thermodynamic stability of polymer crystals. In case of lamellae-crystals, a properly conformed single chain of certain length is the critical nucleus that initiates the crystallization process and, more important, limits the thickness L of the lamellae crystal, since it mostly grows upon refolding of chains. This is the reason, why polymers with lamellar morphology principally cannot escape from high surface-to-volume ratios and exhibit melting temperatures T_m that are distinctly lower than the thermodynamic equilibrium melting temperature

This is an open access article under the terms of the [Creative Commons Attribution](https://creativecommons.org/licenses/by/4.0/) License, which permits use, distribution and reproduction in any medium, provided the original work is properly cited.

© 2022 The Authors. *Journal of Applied Polymer Science* published by Wiley Periodicals LLC.

T_m^0 . Knowing the energy of the refolded crystal surface, the deviation of T_m from T_m^0 can be calculated from L using the Gibbs–Thomson equation 2–4

Crystals in natural rubber (NR) networks are a good example of this polymer-typical characteristic,⁵ because they form at room temperature only under strain but spontaneously melt when the stretching force is released and the rubber retracts back to its original dimensions. This phenomenon, referred to as strain-induced crystallization (SIC), is intensively studied since its discovery in the 1920s, because it is assumed to be responsible for the outstanding high tensile strength of NR at high elongations.^{6–19}

Lately, an unusually lightly crosslinked variant of NR became known, which forms strain-induced crystals that do not vanish at room temperature.²⁰ Since a fraction of less than 20% strain-induced crystals retains the NR network in a highly elongated shape and it recovers its original shape not before these crystals are melted, it is referred to as shape memory natural rubber (SMNR).^{21,22} This shape memory polymer (SMP) distinguishes itself from most other SMPs by its capability of storing high amounts of strain and mechanical energy as well as by a broadly tunable trigger temperature T_{trig} .^{20–31} T_{trig} correlates with the T_m of the strain-induced crystals and depends on the choice of parameters (e.g., temperature, stretching rate) during crystallization. Besides heat, SMNR can be triggered also by contact to suited liquid or even gaseous solvents,^{29,30} and by applying a certain external mechanical stress perpendicular to the chain orientation of the crystallites.^{26,27,31} Increasing mechanical stress perpendicular to the chain orientation as well as contact to suited solvents were found to cause a decrease of T_m until it underruns room temperature and the crystals finally melt, while stress parallel to this direction has a significant T_m -increasing effect. These findings raised the assumption that the stability of crystals in SMNR might be strongly affected by the thermodynamic state of the surrounding amorphous phase and the stress exerted on the crystals. A recent work focused on the realization of a shape memory effect for synthetic rubber (IR) – the natural analogue of NR – substantiates this assumption.³² It was found that the T_m of shape-stabilizing crystals in NR can be effectively increased by adding minor amounts of stearic acid (StA). Since StA – one of the impurities in NR^{33,34} – is known to affect the thermal as well as strain-induced crystallization rates of NR and IR networks,^{35–40} but no direct influence of StA on the T_m of poly(cis-1,4-isoprene) crystals was ever reported, this raises the question of the underlying mechanism.

This work aims on better understanding the influence of StA on the T_m of crystals in poly(cis-1,4-isoprene) networks with the intention to generally obtain more

TABLE 1 Differences between poly(cis-1,4-isoprene)s used in this work

	SMR 10	Natsyn 2200
1,4- cis-content (%)	>99.8 ³³	96–98.4 ^{35,41}
StA content (%)	0.15 ⁴⁰	0
M_n (10^6 g mol ⁻¹)	2.8 ⁴²	2.2 ⁴²
PDI (–)	3.80 ⁴²	3.95 ⁴²

information on whether and how the stability of a polymer crystal depends on internal stress in the surrounding amorphous phase. To this end, NR as well as IR were additivated with StA concentrations of up to 10 wt% and subsequently crosslinked to the lowest degree that just causes an infinitely high viscosity of the melt, as defined elsewhere as critical degree of crosslinking.²² The samples were crystallized upon stretching at room temperature (referred to as cold-crystallization) as well as upon stretching at 80°C and subsequent cooling to room temperature (referred to as hot-crystallization). The determined T_m s of the samples were compared with those calculated from X-ray scattering data using the Gibbs–Thomson equation.

2 | EXPERIMENTAL

2.1 | Materials

The polyisoprene rubbers used in this work are synthetic rubber Natsyn 2200, produced by *Goodyear International Corporation* and kindly provided by *Weber & Schaer GmbH & Co. KG*, and Standard Malaysian Rubber 10 (SMR 10), which was kindly provided by *Continental Reifen Deutschland GmbH*. The differences between the poly(cis-1,4-isoprene)s is summarized in Table 1.

Dicumyl peroxide (DCP) was delivered by *Sigma-Aldrich Chemie GmbH* with a purity of 98%. The stearic acid (StA) used in this work was purchased from *Merck KGaA* with a purity of 97%.

2.2 | Sample preparation

IR and NR were mixed with stearic acid (StA) and dicumyl peroxide (DCP) with a heated mastication double roller from *Bühler & Co GmbH* at a temperature of 80°C for 10 to 15 min using a speed of 14 revolutions per minute. Subsequently, the samples were molded to sheets of 60 × 60 mm and thicknesses ranging between 0.4 and 0.7 mm, and cured at 160°C for 30 min using a heating press from *Paul-Otto-Weber Maschinen Apparatebau*

TABLE 2 Composition of NR and IR samples

NR samples		IR samples					
StA (phr)	DCP (phr)	StA (phr)	DCP (phr)	StA (phr)	DCP (phr)	StA (phr)	DCP (phr)
0	0.409	0	0.216	0	0.425	0	0.602
5.02	0.398	0.501	0.204	0.519	0.421	0.506	0.604
9.99	0.399	1.011	0.197	0.998	0.392	1.01	0.591
20.05	0.402	1.513	0.215	1.508	0.409	1.491	0.605
35.01	0.407	1.999	0.209	1.998	0.404	1.992	0.608
		5.031	0.198	5.053	0.397	5.011	0.619
		10.063	0.196	10.014	0.404	10.003	0.598

GmbH. Shouldered test bars type S3 A (DIN 53504) were stamped from sheets. The compositions of the prepared IR and NR samples are listed in parts per hundred rubber (phr) in Table 2.

2.3 | Crystallization procedure and shape memory parameters

The crystals that are capable of retaining the IR as well as NR samples in a highly elongated temporary shape were strain-induced crystallized upon stretching to 95% of the predetermined fracture strain ε_{95} with a stretching rate of $200\% \text{ s}^{-1}$. In the following, strain-induced crystallization upon stretching at room temperature or 80°C is referred to as cold-crystallization or hot-crystallization, respectively. Before the stretching force was released and the fixed strain $\varepsilon_{f,n}$ was determined, all samples were cooled to 0°C and kept constrained at this temperature for at least 60 s to avoid premature melting and triggering of the sample. Then, the samples were triggered upon heating to 80°C with a heating rate of 1 K min^{-1} and the permanent shape $\varepsilon_{p,n}$ was determined. The recovery ratio R_r and fixity ratio R_f were calculated using the following Equation 1 and 2:

$$R_r(n) = \frac{\varepsilon_{95} - \varepsilon_{p,n}}{\varepsilon_{95} - \varepsilon_{p,n-1}} \cdot 100\% \quad (1)$$

$$R_f(n) = \frac{\varepsilon_{f,n}}{\varepsilon_{95}} \cdot 100\% \quad (2)$$

2.4 | Sample characterization

Measuring of the crystallization temperature T_c and melting temperature T_m of StA crystals in IR and NR networks was carried out with a DSC2910 from TA

Instruments using sample weights of about 10 mg and a heating rate of 10 K min^{-1} .

A dynamic thermomechanical analyzer DMA2980 (TA Instruments, Inc.) was used to determine the degree of crosslinking x_c (fraction of crosslinked repeating units) of the differently crosslinked networks. To this end, the samples were mounted to the film tension clamp and analyzed at 30°C using the controlled-force mode with a preload force of 0.01 N, a frequency of 1 Hz, and an amplitude of $10 \mu\text{m}$. The elongation λ was measured while the force was increased with a ramp of 0.01 N min^{-1} to a maximum force of 18 N. The determined data were evaluated according to Mooney-Rivlin (Equation 3),^{43,44}

$$\sigma \left(\lambda - \frac{1}{\lambda^2} \right)^{-1} = \left(2C_1 + \frac{2C_2}{\lambda} \right), \quad (3)$$

where σ is the stress, and C_1 and C_2 are constants, which were obtained by plotting the left side of Equation 3 against λ^{-1} . The degree of crosslinking was calculated according to Equation 4:⁴⁵

$$x_c = \frac{2M_{\text{rep}}(C_1M_n - \rho RT)}{\rho RTM_n} \cdot 100\%, \quad (4)$$

Here, M_{rep} is the molecular weight of the repeating unit (66.12 g mol^{-1}), M_n the number average molecular weight of the starting polymer (see Table 1), ρ the density (0.93 g cm^{-3}), R the universal gas constant ($8.314 \text{ J mol}^{-1} \text{ K}^{-1}$) and T the temperature.

The solubility of StA in rubber was modeled using the Flory diluent model (Equation 5) assuming an equal density of StA (0.94 g cm^{-3}) and poly(cis-1,4-isoprene) (0.93 g cm^{-3}):^{46,47}

$$1 - \frac{T_m}{T_m^0} = \frac{R}{H_m^0} (D + ET_m) (1 - \varphi_2)^2 \quad (5)$$

Here, T_m^0 is the melting temperature of pure StA (69.5°C), R the universal gas constant (8.314 J mol⁻¹ K⁻¹), H_m^0 the standard enthalpy of fusion of StA (158.99 J g⁻¹) and φ_2 the volume fraction of the fatty acid.^{48,49} D and E are fitting parameters with the values 17.490 and -0.051, respectively, for melting, and 17.725 and -0.0523 for crystallization, respectively.

Wide-angle X-ray scattering (WAXS) patterns were recorded with a VANTEC-2000 detector (Bruker AXS GmbH) using a micro focus X-ray source (I μ S, Incoatec GmbH) with Cu α -anode and integrated Montel Optic operated at 50 kV and 600 μ A (Bruker Nanostar). The X-ray wavelength was 1.5406 Å and the diffraction patterns were recorded in a sample-to-detector distance of 13.25 cm using an accumulation time of 7200 s. The melting process of the samples was monitored using a heatable sample holder. To this end, the samples were stored under liquid nitrogen directly after crystallization to avoid premature melting. In order to allow retraction of the sample upon heating, the samples were fixed only at one side in the precooled sample holder. All samples were measured starting at 0°C and the temperature was increased in steps of 1 K until all crystal reflections disappeared. The lamellar thickness L of the poly(cis-1,4-isoprene) crystals was calculated from the full width at half maximum $\Delta(2\theta_{(002)})$, according to the Scherrer equation (Equation 6):⁵⁰

$$L = \frac{K \lambda}{\Delta(2\theta_{(002)}) \cdot \cos(\theta_{(002)})} \quad (6)$$

The shape factor K was assumed as 0.9, the X-ray wavelength λ was 0.154056 nm and the Bragg-angle 2θ of the (002) reflection plane is 21.94°. The samples were tilted by an angle of 11° to the incident X-ray beam to detect the full-width-at-half-maximum $\Delta(2\theta_{(002)})$ of the (002) reflection at a 2θ position of 21.94°.

The determined lamellar thicknesses L were used for calculating the melting temperatures $T_{m,calc}$ of the poly(cis-1,4-isoprene) crystals according to the Gibbs-Thomson equation (Equation 7),²⁻⁴ using a free surface energy σ of 0.0244 J m⁻²,⁵¹ an equilibrium enthalpy of fusion ΔH_m^0 of 6.4×10^7 J m³,⁵² and an equilibrium melting temperature T_m^0 of 35.5°C.⁵¹

$$T_{m,calc} = T_m^0 - \frac{2\sigma T_m^0}{\Delta H_m^0 \cdot L} \quad (7)$$

Besides calculating the melting temperature from WAXS data, T_m was also measured indirectly. To this end, the retraction process of the differently crystallized IR and NR, which takes place in a certain temperature range

when the samples are heated, was taken as indicator for the melting of the strain-stabilizing poly(cis-1,4-isoprene) crystals. The retraction of the samples was monitored via the thickness increase of the samples with a thermomechanical analyzer TMA 2940 (TA Instruments, Inc.), heated with a heating rate of 1 K min⁻¹ while applying a preload force of 0.05 N. The average trigger temperature T_{trig} , which is shown in the manuscript to correlate with the average melting temperature of the poly(cis-1,4-isoprene) crystals, was determined at the inflection point of the recorded thickness vs. temperature plot as described elsewhere.²⁰

3 | RESULTS AND DISCUSSION

Goal of this work was to get insights into the influence of StA and the internal stress on the T_m of crystals in poly(cis-1,4-isoprene). To this end, additive-free synthetic rubber Natsyn 2200 (IR) as well as natural rubber SMR 10 (NR) were mixed with StA concentrations c_{StA} of up to 9 wt%, and subsequently crosslinked with dicumyl peroxide (DCP). We chose to crosslink the samples to a critical degree of crosslinking, an unusual lightly crosslinking of a thermoplastic right at the borderline where its viscosity just becomes infinite. This was decided because critical crosslinking only weakly affects the crystallizability of the samples. Thus, different amounts of DCP were used to prepare IR and NR networks of different degrees of crosslinking x_c and to find out the needed DCP concentration $c_{DCP,crit}$ for this purpose. $c_{DCP,crit}$ and, thus, the maximum strain ϵ_{max} of IR and NR were found to be unaffected by StA, even by incorporation of StA up to 9 wt%. The degrees of critical crosslinking $x_{c,crit}$ of IR and NR were determined to 0.23% and 0.22%, respectively (Table 3), which is in good accordance with the literature.²⁰

Regarding the shape memory effect, which is accompanied with critical crosslinking of the differently StA-additivated IR and NR samples, it was found that except of the trigger temperature T_{trig} all other shape-memory relevant properties are also unaffected by the incorporated amount of StA. The maximum strain ϵ_{max} , fixity ratio R_f and recovery ratio R_r were found to be constant over at least 3 cycles and are listed in Table 3. The expectedly different average trigger temperatures T_{trig} of cold- as well as hot-crystallized critically crosslinked IR and NR are shown in dependence on c_{StA} in Figure 1.

All measured T_{trig} s of cold- and hot-crystallized NR networks are higher compared to the respective IR networks with similar StA contents. This can be explained by the poorer stereoregularity of IR compared to NR and the corresponding lower probability of forming thicker

lamellae crystals with higher melting temperatures. Nevertheless, the T_{trig} s of both, NR as well as IR networks, expectedly increase with increasing c_{StA} , according to findings in an earlier work.³² The highest applied c_{StA} results in the highest T_{trig} , being 23.2 and 20.1 °C for cold-crystallized NR and IR, respectively, and 38.9 and 25.6 °C for hot-crystallized NR and IR networks, respectively.

Since it is possible that T_{trig} correlates with the melting temperature of StA crystals above a certain concentration of StA in IR and NR networks as reported elsewhere,^{32,53–55} we measured and calculated the melting and crystallization temperatures of StA crystals in the following to ensure that this is not the case here. The melting temperature $T_{\text{m,StA}}$ as well as the crystallization temperature $T_{\text{c,StA}}$ of StA crystals in the rubber samples

TABLE 3 DCP concentration needed for critical crosslinking $c_{\text{DCP,crit}}$, critical degree of crosslinking $x_{\text{c,crit}}$ and resulting maximum strain ϵ_{max} of IR and NR samples

	IR	NR
$c_{\text{DCP,crit}}$ (wt%)	0.20 ± 0.01	0.40 ± 0.01
$x_{\text{c,crit}}$ (%)	0.23 ± 0.08	0.22 ± 0.08
ϵ_{max} (%)	1400 ± 10	1400 ± 10
R_f (%)	90 ± 2	90 ± 2
R_r (%)	95 ± 2	95 ± 2

FIGURE 1 Average trigger temperature T_{trig} of critically crosslinked NR- and IR-networks in dependence on StA concentration c_{StA} and crystallization temperature. (a) Cold-crystallized at 20 °C, (b) hot-crystallized at 80 °C

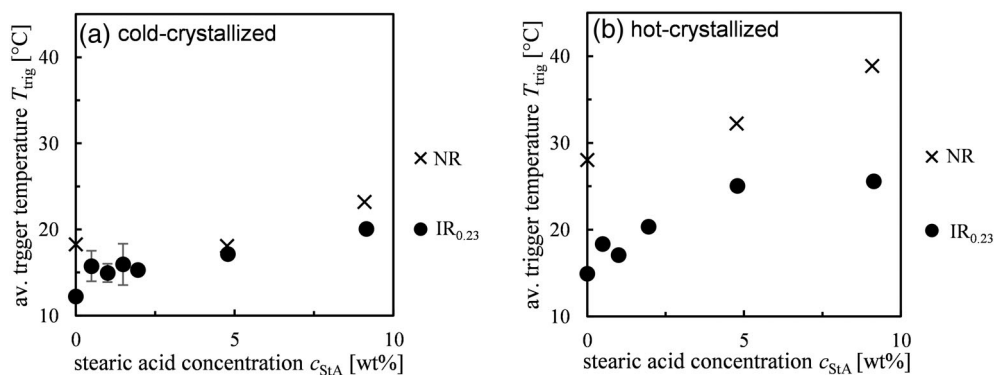
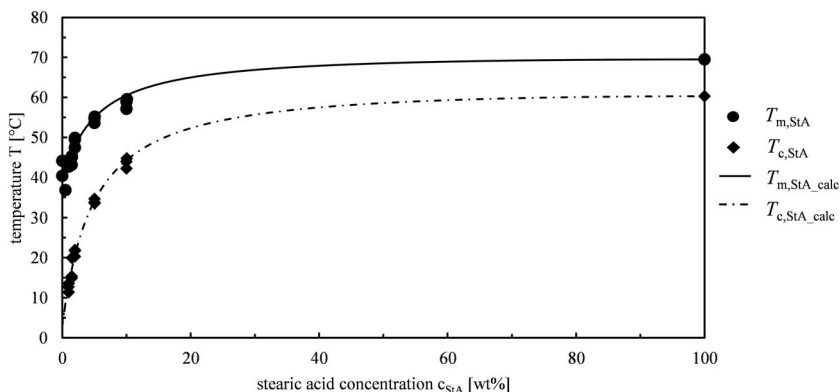


FIGURE 2 Melting temperature $T_{\text{m,StA}}$ and crystallization temperature $T_{\text{c,StA}}$ of StA crystals in IR samples in dependence on StA concentration c_{StA} . Lines indicate the melting temperature $T_{\text{m,StA_calc}}$ and crystallization temperature $T_{\text{c,StA_calc}}$, calculated according to Flory's diluent model



were found independent of the degree of crosslinking and kind of rubber, but expectedly dependent on c_{StA} . Figure 2 shows the determined $T_{\text{m,StA}}$ and $T_{\text{c,StA}}$ in dependence on c_{StA} representatively for IR samples. Both, $T_{\text{m,StA}}$ as well as $T_{\text{c,StA}}$ fit well the curves of the calculated melting and crystallization temperatures, $T_{\text{m,StA_calc}}$ and $T_{\text{c,StA_calc}}$, according to Flory's diluent model.^{46,47}

All measured as well as calculated melting temperatures of StA, $T_{\text{m,StA}}$ and $T_{\text{m,StA_calc}}$, respectively, were found to be fairly above the determined T_{trig} s (see Figure 1) of the respective hot- as well as cold-crystallized IR and NR networks. This confirms that the SME of IR and NR networks up to a c_{StA} of 9 wt% is not based on the StA crystals. Thus, the SME of IR and NR samples with StA up to 9 wt% is related to the poly(cis-1,4-isoprene) crystals and the incorporated StA obviously influences T_{trig} and, accordingly, T_{m} of these crystals.

In the following, we focus on exploring the melting process of the strain-stabilizing poly(cis-1,4-isoprene) crystals in the StA additivated IR and NR networks. Unfortunately, DSC is not suited for this purpose since superposition of the relaxation enthalpy with the heat of fusion of the crystals, as well as movement of the retracting sample will cause defective heat flows and prevent from any reliable evaluation. Alternatively, we chose to carry out WAXS experiments and monitored the intensities of the basal (200) reflections of the poly(cis-

1,4-isoprene) crystals as indicator for the crystallinity of the differently composed samples at certain temperatures. Figure 3 exemplarily shows the measured (200) intensities for a cold- and a hot-crystallized IR sample with a c_{StA} of 1% in dependence on temperature. The trigger process of identical samples was measured by monitoring the thickness increase upon heating with a TMA, as explained elsewhere,²⁶ and combined with the measured (200) intensities in Figure 3. We found for all samples, that the (002) intensity decreases with increasing temperature, while the sample thickness simultaneously

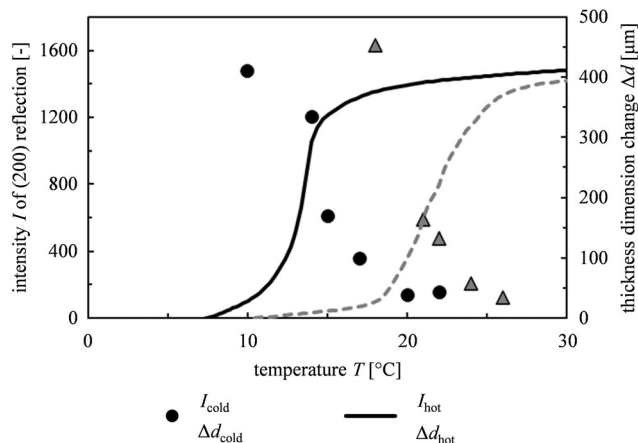


FIGURE 3 Intensity I of the (200) reflection of poly(cis-1,4-isoprene) crystals and recovery ratio R_r versus temperature of a cold- and a hot-crystallized IR with an StA concentration of 1%

increases. The biggest change of intensity takes place at the same temperature where the thickness changes the most, which is T_{trig} by definition.

This behavior was found for all cold- as well as hot-crystallized, differently StA additivated IR and NR samples and confirms that triggering of the SME is solely related with the melting of the poly(cis-1,4-isoprene) crystals even after adding StA up to 9 wt%. Thus, T_{trig} is truly equal to T_m of the crystals in IR and NR and the StA concentration actually influences T_m of the polymer crystals.

Following the assumptions of earlier works that internal stress may strongly affect T_m of the crystals and the shape-memory effect of NR and IR,³² we continued with measuring T_m in dependence on the amount of incorporated StA and the kind of crystallization. Since, as mentioned above, direct measuring by DSC is not possible for this task, we alternatively obtained information about the lamellar thicknesses L of crystals in IR and NR samples from the full-width-at-half maximum $\Delta(2\theta_{(002)})$ of the (002) reflection (equation 6) and calculated the corresponding melting temperature $T_{m,\text{calc}}$ according to Gibbs–Thomson (equation 7).

Figure 4 representatively shows the measured T_{trig} (= $T_{m,\text{meas}}$) and the calculated $T_{m,\text{calc}}$ for cold- as well as hot-crystallized IR and NR samples in dependence on c_{StA} . In contrast to the measured $T_{m,\text{meas}}$ the calculated $T_{m,\text{calc}}$ of crystals in NR as well as IR samples are found nearly independent of the amount of incorporated StA,

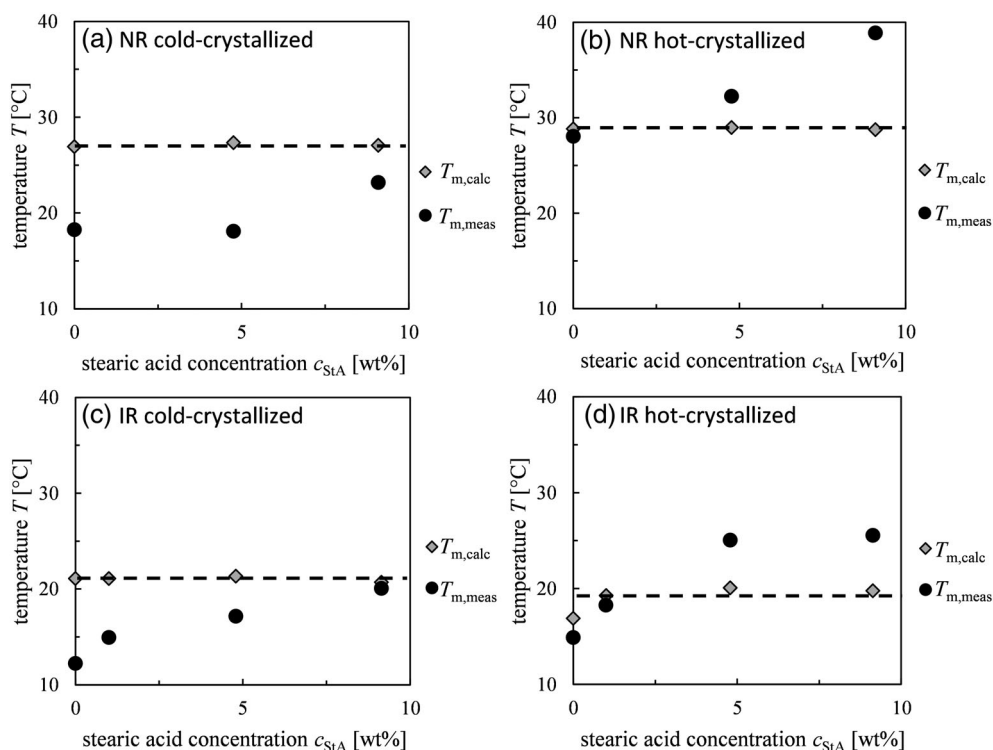


FIGURE 4 Comparison of calculated melting temperature $T_{m,\text{calc}}$ and measured trigger temperature $T_{m,\text{meas}}$ of IR and NR samples in dependence on stearic acid concentration c_{StA} and kind of crystallization

that is, the lamellar thickness of the polymer crystals is not affected by StA. Also, the kind of crystallization has no significant influence on the $T_{m,calc}$ of IR and NR, which were determined for cold-crystallized samples to $27.1 \pm 0.2^\circ\text{C}$ and for hot-crystallized samples to $28.8 \pm 0.1^\circ\text{C}$. The same was found for IR samples but with distinctly lower $T_{m,calc}$ of $21.1 \pm 0.4^\circ\text{C}$ for cold-crystallized and $19.1 \pm 2.1^\circ\text{C}$ for hot-crystallized samples. Although the higher $T_{m,calc}$ of crystals in NR can be explained by the higher stereoregularity of the poly(cis-1,4-isoprene) chains, which allows formation of potentially thicker lamellae crystals,^{33,35,38,41} the measured $T_{m,meas}$ highly deviate from the calculated $T_{m,calc}$.

Regarding the deviation of $T_{m,meas}$ from $T_{m,calc}$ reveals for cold-crystallized IR as well as NR samples that $T_{m,meas}$ is invariably lower than the calculated $T_{m,calc}$ but converges against $T_{m,calc}$ with increasing StA concentration (Figure 4a,c). In case of hot-crystallized IR and NR samples, $T_{m,meas}$ fits well $T_{m,calc}$ in samples without StA but increasingly exceeds it with increasing content of added StA (Figure 4b,d).

Although the T_m -influencing dimensions of the crystals in IR or NR samples and, thus, the calculated melting temperatures $T_{m,calc}$ are nearly constant and neither influenced by the kind of crystallization nor the content of added StA, the measured melting temperatures $T_{m,meas}$ depend on both and strongly deviate from $T_{m,calc}$. Based on the findings of previous works that mechanical stressing of a cold-crystallized NR sample results in internal stress onto the crystals, which can cause an increase as well as decrease of T_m dependent on its direction, we hypothesize that the deviation between $T_{m,meas}$ and $T_{m,calc}$ is caused by internal stress onto the strain-stabilizing crystals. We assume that the retraction forces of the strained macromolecules in the surrounding amorphous phase are responsible for this stress and that this stress is somehow influenced by the added StA. The fact that $T_{m,meas}$ deviates up- as well as downward from $T_{m,calc}$ might be explained by the general anisotropy of a polymer crystal, as illustrated in Figure 5. Internal tensile stress along as well as compressive stress perpendicular to the macromolecular chain direction (Figure 5a) might support the thermodynamic stability of a polymer crystal and increase its T_m above $T_{m,calc}$, while compressive stress along as well as tensile stress perpendicular to the chain direction (Figure 5b) might destabilize a polymer crystal and decrease its T_m below $T_{m,calc}$.

Taking a closer look at the WAXS patterns of differently crystallized IR and NR samples with added StA concentration between 1 and 9 wt% shows besides the reflections of the poly(cis-1,4-isoprene) crystals also reflections of StA crystals (see Figure 6). This indicates that StA is not completely dissolved in the amorphous

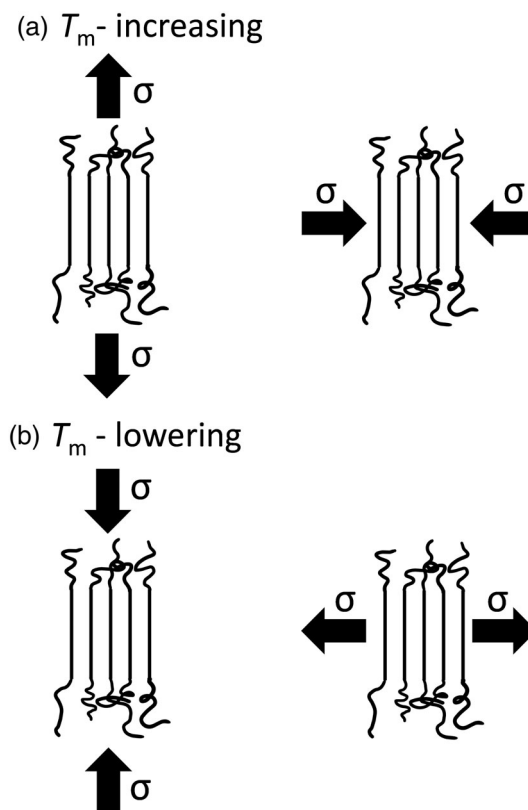


FIGURE 5 Assumed effect of internal stress σ on the melting temperature T_m of a polymer crystal differentiated by kind and direction

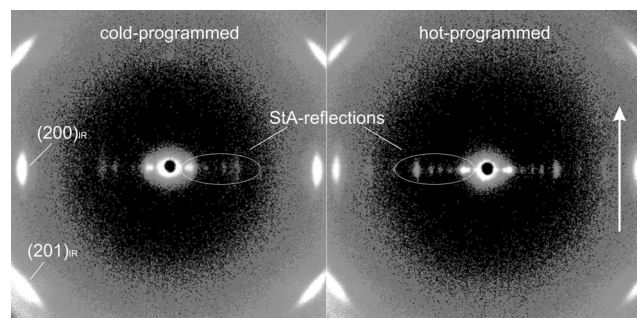


FIGURE 6 Representative WAXS patterns of 5 wt% StA containing cold- (left) and hot-crystallized (right) IR samples with reflections of StA crystals. The arrow indicates the stretching direction

phase of IR and NR samples and forms crystals, even at small concentrations of 1 wt%.

Based on these findings, the discrepancy between the measured lower and higher $T_{m,meas}$ compared to the calculated, dimension-related $T_{m,calc}$ might be explained as follows:

In the case of cold-crystallization, the StA crystals are already present and evenly distributed in the relaxed amorphous IR or NR samples. Upon stretching, the

Cold-crystallization

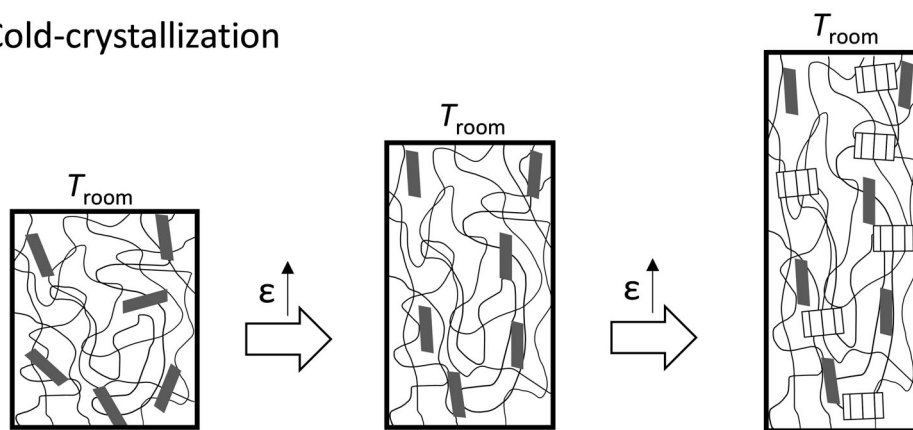
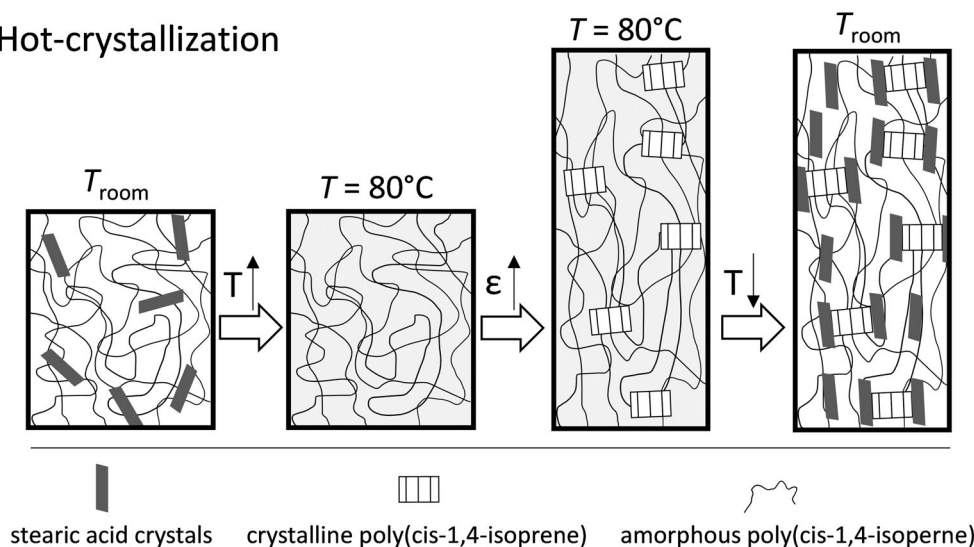


FIGURE 7 Formation and arrangement of poly(cis-1,4-isoprene) and StA crystals during cold- and hot-crystallization of crosslinked NR and IR samples

Hot-crystallization



netchains of the amorphous network are increasingly oriented along the applied strain direction. This, however, causes also an orientation of the embedded StA crystals, as seen in Figure 5. Tosaka et al. reported that the StA crystals are already highly oriented before poly(cis-1,4-isoprene) crystals are formed upon strain-induced crystallization (SIC).⁵⁶ Further, it is reported that the formation of strain-induced crystals causes partial relaxation of the surrounding amorphous phase.^{56–58} In the case of critically crosslinked IR and NR networks, the strain-induced crystallization obviously results in a T_m fairly above room temperature but below the corresponding $T_{m,calc}$. We assume that this is due to a T_m -lowering stress (see Figure 6) on the strain-stabilizing poly(cis-1,4-isoprene) crystals, which is caused by the entropy-driven retraction force of macromolecules in the surrounding amorphous phase. Oriented StA crystals in the amorphous phase possibly reduce this internal T_m -lowering stress on the poly(cis-1,4-isoprene) crystals by interfering the retraction of the surrounding amorphous phase. Thus, the more StA is incorporated in the

amorphous phase, the more the observed $T_{m,meas}$ converges against the calculated $T_{m,calc}$.

In the case of hot-crystallization, we suppose that the scenario between StA and poly(cis-1,4-isoprene) crystals is reversed. As indicated by the findings of Heuwers et al., poly(cis-1,4-isoprene) crystals do not melt even at temperatures well above 80°C as long the sample is kept constrained at high elongation.^{26,27} Thus, we deduce that SIC of poly(cis-1,4-isoprene) crystals even takes place at a temperature of 80°C and that StA is the second to crystallize during cooling to room temperature due to its melting temperature below 80°C. The existence of poly(cis-1,4-isoprene) crystals at such high temperature might be explained as follows. The applied external stretching force causes a T_m -increasing internal stress on the crystals, which shifts $T_{m,meas}$ fairly above 80°C. Releasing the stretching force at such a high temperature would instantly lower the T_m -increasing stress followed by immediate melting and full retraction of the sample. Keeping the sample constrained while cooling to room temperature causes the crystallization of StA. The formed

StA crystals are obviously capable of turning the stress exerted by the amorphous phase on the crystals towards a T_m -increasing one, resulting in a $T_{m,meas}$ equal or even higher than $T_{m,calc}$ in dependence on the amount of incorporated StA. This hypothesis is supported by the WAXS pattern of the hot-crystallized IR sample containing 5 wt% StA in Figure 5 (right), which indicates the StA crystals are as highly oriented as the poly(cis-1,4-isoprene) crystals. Since StA is known to nucleate the thermal crystallization of poly(cis-1,4-isoprene) crystals,³⁶ we assume that in case of hot-crystallization the reverse takes place and the poly(cis-1,4-isoprene) crystals nucleate the StA crystals, which take over the orientation of the poly(cis-1,4-isoprene) crystals in the sense of an epitaxy.^{36,59,60} If this holds true, StA crystals would stay in direct contact to the nucleation sites of the poly(cis-1,4-isoprene) crystals and decorate their (hk0) crystal surfaces. These StA crystals in direct contact to the poly(cis-1,4-isoprene) crystals might act similar to a corset, that stabilizes the crystals and cushions them against T_m -lowering stress from the surrounding amorphous phase. The presumed different roles of StA crystals in cold- and hot-crystallized NR and IR samples are depicted in Figure 7.

4 | CONCLUSION

Exploring the influence of StA on the melting temperature T_m of strain-induced crystallized IR and NR networks showed that the T_m of the poly(cis-1,4-isoprene) crystals strongly deviates up- as well as downward from the crystal dimension-related, calculated melting temperature $T_{m,calc}$ in dependence on the amount of added StA and the selected crystallization conditions. Strain-induced crystallization at room temperature causes a T_m significantly smaller than $T_{m,calc}$ that increases with increasing amount of StA until it fits $T_{m,calc}$ at an StA concentration of 9 wt%. Strain-induced crystallization at 80°C initially causes a T_m nearly equal to $T_{m,calc}$ that increasingly exceeds $T_{m,calc}$ with increasing amount of added StA.

Supported by the phenomena of stress-induced melting and stress-induced stabilization, we hypothesize internal stress exerted onto the crystals by the surrounding amorphous phase as responsible for the observed discrepancy between T_m and $T_{m,calc}$. It is assumed that the direction and intensity of this internal stress depends on the crystallization conditions and can be influenced by the amount and the location of StA crystals in the amorphous phase.

In summary, this points out that the melting temperature of polymer crystals does not only depend on

surface-to-volume effects but is also strongly affected by internal stress exerted by the surrounding amorphous phase. Since this stress seems to be effectively influenceable by additives towards a T_m even above $T_{m,calc}$, future work will focus on verifying these findings for other polymers and on proving this as a potential opportunity to stabilize polymer crystals towards melting temperatures beyond their usual melting temperatures.

AUTHOR CONTRIBUTIONS

Dominik Segiet: Conceptualization (equal); investigation (equal); writing – original draft (equal); writing – review and editing (equal). **Sebastian Weckes:** Investigation (equal). **Juergen Austermuehl:** Investigation (equal). **Joerg C. Tiller:** Supervision (supporting). **Frank Katzenberg:** Conceptualization (lead); investigation (equal); writing – original draft (lead); writing – review and editing (lead).

ACKNOWLEDGMENT

Open Access funding enabled and organized by Projekt DEAL.

DATA AVAILABILITY STATEMENT

The data that support the findings of this study are available from the corresponding author upon reasonable request.

ORCID

Frank Katzenberg  <https://orcid.org/0000-0001-6585-5534>

REFERENCES

- [1] P. J. Flory, *J. Chem. Phys.* **1949**, *17*, 223.
- [2] J. D. Hoffman, J. J. Weeks, *J. Res. Nbs A Phys. Chem.* **1962**, *66*, 13.
- [3] J. I. Lauritzen, J. D. Hoffman, *J. Chem. Phys.* **1959**, *31*, 1680.
- [4] J. I. Lauritzen, J. D. Hoffman, *J. Res. Nbs A Phys. Chem.* **1960**, *64*, 73.
- [5] W. Bai, J. Guan, H. Liu, S. Cheng, F. Zhao, S. Liao, *Polymers* **2021**, *13*, 4306.
- [6] J. Katz, *Chem. Ztg.* **1925**, *49*, 353.
- [7] J. Katz, *Trans. Faraday Soc.* **1936**, *32*, 77.
- [8] P. Z. Chen, J. Y. Zhao, Y. F. Lin, J. R. Chang, L. P. Meng, D. L. Wang, W. Chen, L. Chen, L. B. Li, *Soft Matter* **2019**, *15*, 734.
- [9] Q. Demassieux, D. Berghezan, S. Cantournet, H. Proudhon, C. Creton, *J. Polym. Sci. Part B-Polym. Phys.* **2019**, *57*, 780.
- [10] A. Gros, B. Huneau, E. Verron, M. Tosaka, *J. Mech. Phys. Solids* **2019**, *125*, 164.
- [11] Y. Kitamura, K. Okada, H. Masunaga, M. Hikosaka, *Polym. J.* **2019**, *51*, 221.
- [12] P.-A. Albouy, P. Sotta, *Macromolecules* **2020**, *53*, 992.
- [13] P. Sotta, P. A. Albouy, *Macromolecules* **2020**, *53*, 3097.

- [14] N. Candau, O. Oguz, C. E. Federico, G. Stoclet, J.-F. Tahon, M. L. MasPOCH, *Polym. Test.* **2021**, *101*, 107313.
- [15] C. B. Zhang, C. Liu, L. Wang, Y. Zhao, G. M. Liu, D. J. Wang, *Chem. Commun.* **2021**, *58*, 286.
- [16] J. Zhao, S. Feng, W. Zhang, W. Chen, J. Sheng, W. Yu, L. Li, *Macromolecules* **2021**, *54*, 9204.
- [17] J.-B. Le Cam, A. Tayeb, S. Charlès, *Polymer* **2022**, *255*, 125120.
- [18] R. Osumi, T. Yasui, R. Tanaka, T.-T. Mai, H. Takagi, N. Shimizu, K. Tsunoda, S. Sakurai, K. Urayama, *ACS Macro Lett.* **2022**, *11*, 747.
- [19] X. Qi, L. Wang, Y. Zhang, M. Jia, L. Zhang, D. Yue, *Macromolecules* **2022**, *55*, 2758.
- [20] B. Heuwers, A. Beckel, A. Krieger, F. Katzenberg, J. C. Tiller, *Macromol. Chem. Phys.* **2013**, *214*, 912.
- [21] F. Katzenberg, B. Heuwers, J. C. Tiller, *Adv. Mater.* **2011**, *23*, 1909.
- [22] F. Katzenberg, J. C. Tiller, *J. Polym. Sci., Part B: Polym. Phys.* **2016**, *54*, 1381.
- [23] W. Voit, T. Ware, R. R. Dasari, P. Smith, L. Danz, D. Simon, S. Barlow, S. R. Marder, K. Gall, *Adv. Funct. Mater.* **2010**, *20*, 162.
- [24] P. T. Mather, X. Luo, I. A. Rousseau, *Annu. Rev. Mater. Res.* **2009**, *39*, 445.
- [25] R. Hoehner, T. Raidt, M. Rose, F. Katzenberg, J. C. Tiller, *J. Polym. Sci., Part B: Polym. Phys.* **2013**, *51*, 1033.
- [26] B. Heuwers, D. Quitmann, F. Katzenberg, J. C. Tiller, *Macromol. Rapid Commun.* **2012**, *33*, 1517.
- [27] B. Heuwers, D. Quitmann, R. Hoehner, F. M. Reinders, S. Tiemeyer, C. Sternemann, M. Tolan, F. Katzenberg, J. C. Tiller, *Macromol. Rapid Commun.* **2013**, *34*, 180.
- [28] M. Anthamatten, S. Roddecha, J. Li, *Macromolecules* **2013**, *46*, 4230.
- [29] D. Quitmann, N. Gushterov, G. Sadowski, F. Katzenberg, J. C. Tiller, *ACS Appl. Mater. Interfaces* **2013**, *5*, 3504.
- [30] D. Quitmann, N. Gushterov, G. Sadowski, F. Katzenberg, J. C. Tiller, *Adv. Mater.* **2014**, *26*, 3441.
- [31] D. Quitmann, M. Dibolik, F. Katzenberg, J. C. Tiller, *Macromol. Mater. Eng.* **2015**, *300*, 25.
- [32] D. Segiet, L. M. Neuendorf, J. C. Tiller, F. Katzenberg, *Polymer* **2020**, *203*, 122788.
- [33] Y. Tanaka, S. Kawahara, J. Tangpakdee, *Kautsch. Gummi Kunstst.* **1997**, *50*, 6.
- [34] L. Tarachiwin, J. Sakdapipanich, K. Ute, T. Kitayama, Y. Tanaka, *Biomacromolecules* **2005**, *6*, 1858.
- [35] D. R. Burfield, *Polymer* **1984**, *25*, 1823.
- [36] S. Kohjiya, M. Tosaka, M. Furutani, Y. Ikeda, S. Toki, B. S. Hsiao, *Polymer* **2007**, *48*, 3801.
- [37] S. Kawahara, N. Nishiyama, T. Kakubo, Y. Tanaka, *Rubber Chem. Technol.* **1996**, *69*, 600.
- [38] A. N. Gent, S. Kawahara, J. Zhao, *Rubber Chem. Technol.* **1998**, *71*, 668.
- [39] T. Kakubo, A. Matsuura, S. Kawahara, Y. Tanaka, *Rubber Chem. Technol.* **1998**, *71*, 70.
- [40] S. Kawahara, T. Kakubo, J. T. Sakdapipanich, Y. Isono, Y. Tanaka, *Polymer* **2000**, *41*, 7483.
- [41] M. J. Shuttleworth, A. A. Watson, In *Developments in Rubber Technology—2: Synthetic Rubbers* (Eds: A. Whelan, K. S. Lee), Springer, Netherlands **1981**.
- [42] W. S. Fulton, S. A. Groves, *J. Nat. Rubber Res.* **1997**, *12*, 154.
- [43] M. Mooney, *J. Appl. Phys.* **1940**, *11*, 582.
- [44] R. S. Rivlin, *Philos. Trans. R. Soc., A* **1948**, *241*, 379.
- [45] M. Gordon, *Br. Polym. J.* **1976**, *8*, 39.
- [46] M. L. Huggins, *J. Am. Chem. Soc.* **1942**, *64*, 1712.
- [47] P. J. Flory, *Principles of Polymer Chemistry*, Cornell University Press, New York **1953**.
- [48] N. D. Lebedeva, *Russ. J. Phys. Chem.* **1964**, *38*, 1435.
- [49] N. Garti, E. Wellner, S. Sarig, *Krist. Tech.* **1980**, *15*, 1303.
- [50] P. Scherrer, *Göttinger Nachr. Gesell.* **1918**, *2*, 98.
- [51] E. Dalal, K. D. Taylor, P. J. Phillips, *Polymer* **1983**, *24*, 1623.
- [52] H. g. Kim, L. Mandelkern, *J. Polym. Sci. Part A-2: Polym. Phys.* **1972**, *10*, 1125.
- [53] N. R. Brostowitz, R. A. Weiss, K. A. Cavicchi, *ACS Macro Lett.* **2014**, *3*, 374.
- [54] K. A. Cavicchi, *Macromol. Symp.* **2015**, *358*, 194.
- [55] M. Pantoja, Z. Lin, M. Cakmak, K. A. Cavicchi, *J. Polym. Sci., Part B: Polym. Phys.* **2018**, *56*, 673.
- [56] M. Tosaka, S. Murakami, S. Poompradub, S. Kohjiya, Y. Ikeda, S. Toki, I. Sics, B. S. Hsiao, *Macromolecules* **2004**, *37*, 3299.
- [57] Y. Miyamoto, H. Yamao, K. Sekimoto, *Macromolecules* **2003**, *36*, 6462.
- [58] B. Amram, L. Bokobza, J. P. Queslel, L. Monnerie, *Polymer* **1986**, *27*, 877.
- [59] J. C. Wittmann, B. Lotz, *Prog. Polym. Sci.* **1990**, *15*, 909.
- [60] J. Petermann, Y. Xu, *J. Mater. Sci.* **1991**, *26*, 1211.

How to cite this article: D. Segiet, S. Weckes, J. Austermeuhl, J. C. Tiller, F. Katzenberg, *J. Appl. Polym. Sci.* **2022**, *139*(46), e53146. <https://doi.org/10.1002/app.53146>